

# RSC Advances



This is an *Accepted Manuscript*, which has been through the Royal Society of Chemistry peer review process and has been accepted for publication.

*Accepted Manuscripts* are published online shortly after acceptance, before technical editing, formatting and proof reading. Using this free service, authors can make their results available to the community, in citable form, before we publish the edited article. This *Accepted Manuscript* will be replaced by the edited, formatted and paginated article as soon as this is available.

You can find more information about *Accepted Manuscripts* in the [Information for Authors](#).

Please note that technical editing may introduce minor changes to the text and/or graphics, which may alter content. The journal's standard [Terms & Conditions](#) and the [Ethical guidelines](#) still apply. In no event shall the Royal Society of Chemistry be held responsible for any errors or omissions in this *Accepted Manuscript* or any consequences arising from the use of any information it contains.

***In-situ* photogalvanic acceleration of optofluidic kinetics: a new  
paradigm for advanced photocatalytic technologies †**

Huizhi Wang <sup>a</sup>, Xiaojiao Luo <sup>bd</sup>, Michael K.H. Leung <sup>c</sup>, Dennis Y.C. Leung <sup>b</sup>, Zhiyong Tang <sup>d</sup>,  
Hailiang Wang <sup>e</sup>, Rafael Luque <sup>f</sup>, Jin Xuan <sup>a\*</sup>

<sup>a</sup> School of Engineering and Physical Sciences, Heriot-Watt University, Edinburgh, United Kingdom

<sup>b</sup> Department of Mechanical Engineering, The University of Hong Kong, Pok Fu Lam, Hong Kong

<sup>c</sup> Ability R&D Energy Research Centre, School of Energy and Environment, City University of Hong Kong, Tat Chee Avenue, Kowloon, Hong Kong

<sup>d</sup> CAS Key Laboratory of Low-Carbon Conversion Science and Engineering, Shanghai Advanced Research Institute, Chinese Academy of Sciences, Shanghai 201210, China

<sup>e</sup> Department of Chemistry, Yale University, West Haven, CT, United States

<sup>f</sup> Departamento de Química Orgánica, Universidad de Córdoba, Edif. Marie Curie, Ctra Nnal IV-A, Km 396, E14014 Córdoba, Spain

\*Corresponding Author, Tel: +44 (0) 131 451 3293; Fax: +44 (0)131 451 3129. Email addresses: [j.xuan@hw.ac.uk](mailto:j.xuan@hw.ac.uk) (J. Xuan).

† Electronic supplementary information (ESI) available: Experimental details, UV–vis absorption spectra and a video recording reactor operation.

**Abstract**

A multiscale-designed optofluidic reactor is demonstrated in this work, featuring an overall reaction rate constant of  $1.32 \text{ s}^{-1}$  for photocatalytic decolourization of methylene blue, which is an order of magnitude higher as compared to literature records. A novel performance-enhancement mechanism of microscale *in-situ* photogalvanic acceleration was found to be the main reason for the superior optofluidic performance in the photocatalytic degradation of dyes as model reaction.

Photocatalytic technologies have received increasing attention in a number of important applications including water purification [1], fuel production [2], electricity conversion [3] and environmental monitoring [4]. One major barrier for large-scale application of photocatalytic technologies relates to their inherently slow reaction rates [5-6]. The first generation of batch-type photocatalytic reactors (e.g. annular and slurry reactors) are normally operated in the time-scale of hours with reaction rate constant from  $10^0$  to  $10^2$  hour<sup>-1</sup> and residence times from  $10^0$  to  $10^2$  hour (Fig. 1 (a)) [7 - 12]. The slow performance is mainly due to the insufficient mass and photon transfer (due to the shielding effect of dye solution) in the reaction system [5].

Optofluidics is an emerging field encompassing a synergetic combination of optics/photonics and microfluidics to leverage the specific advantages of both disciplines [5]. Such concept has been proposed in the field of photocatalysis to address the aforementioned challenges present in traditional batch-based systems. With the ability of reactant and light transport intensification at the microscale, the development of second generation of optofluidic reactors in the past decade has remarkably improved overall reaction rate constants to  $10^0 \sim 10^2$  min<sup>-1</sup> and shortened residence times to  $10^0 \sim 10^2$  min (Fig. 1 (b)) [5, 13 - 19]. These processes can be considered virtually free of mass transport constraints as both light and mass transport are intensified under optofluidic conditions. However, these systems are unable to achieve *real-time reactions* (within the second time-scale). Due to these inherent drawbacks, photocatalytic processes still face non trivial limitations for their widespread implementation in applications requiring an instantaneous completion (e.g. continuous monitoring, on-pipe water purification and point-of-care diagnose). Even for such slow reaction rates, an effective large illuminated area is also required, which raises critical cost issues for scale-up systems. Zhang *et al.* [19] recently developed an

optofluidic platform for rapid photocatalytic screening. A typical set of experiment to complete dye degradation plus kinetics required over 10 minutes. Among various tests, the fastest kinetics data on the optofluidic platform (TiO<sub>2</sub>-ZnO catalyst) corresponded to a reaction rate constant of 0.22 min<sup>-1</sup>. This appears to be the highest reported rate constant for an aqueous photocatalytic system.

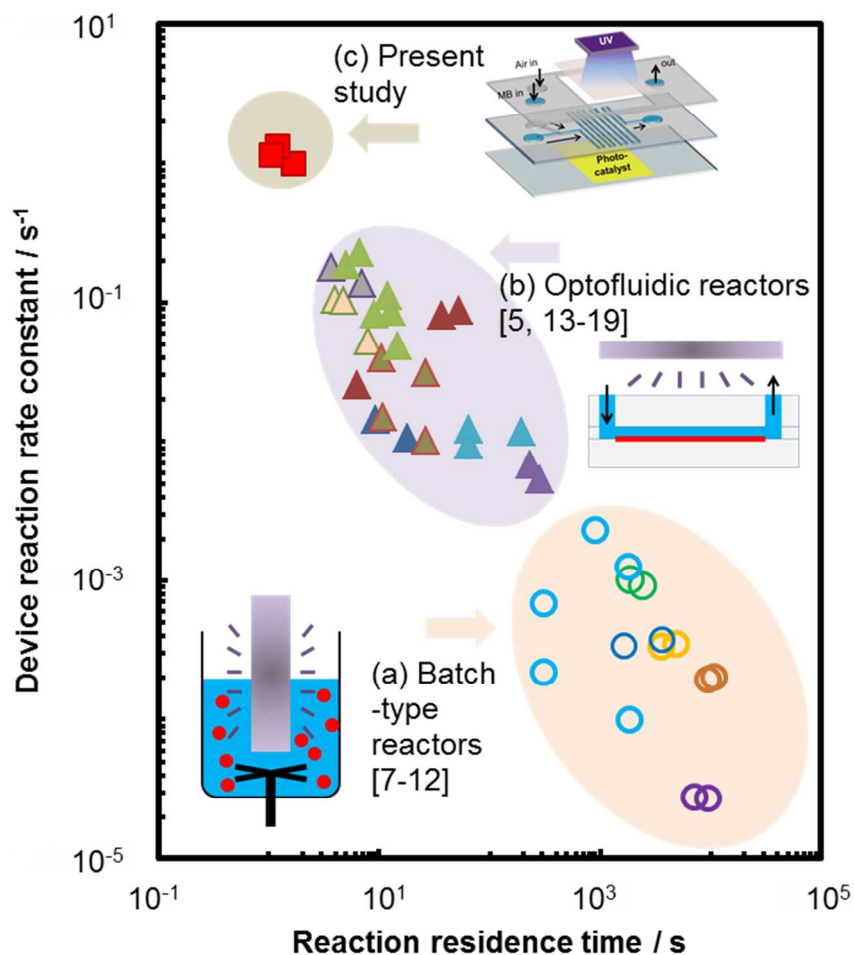


**Fig. 1.** State-of-the-art reactor characteristics. The reaction rate constant and reaction residence time for three generations of aqueous photocatalytic reactors: (a) batch-type photocatalytic reactors, (b) optofluidic reactors, and (c) present study.

Based on fundamental understanding of optofluidic systems, this work was aimed to design a new generation of advanced optofluidic reactors to overcome these constraints and provide ultimate reaction rate constants and residence time in the time-scale of seconds, i.e.,  $> 10^0 \text{ s}^{-1}$  and  $< 10^0 \text{ s}$ , respectively (Fig. 1(c)). In contrast to previous studies in which optofluidics were employed to enhance mass and photon transfer [13-19], the proposed technology is based on a precise control of microscale mass, photon and electron transport, featuring an unprecedented self-powered photogalvanic acceleration mechanism to improve the intrinsic photocatalyst kinetics.

Oxygen is an electron scavenger commonly used in photocatalysis system due to its wide availability and cost-effectiveness. Many photocatalytic systems adopt multiphase flow design by pumping oxygen bubbles into the reactor [20-22], in which light-excited electrons at the conduction band of the semiconductor photocatalyst can be more rapidly consumed, upon enhanced contact with the photocatalytic reactive sites. However, only very limited proportion of reactive site can form the triple-phase boundary benefiting from enhanced kinetics with bubbles generally in the scale of microns (a size which mismatches with the photocatalyst particles at the nanoscale). Comparably, most of the catalyst surface is still under oxygen-starving conditions, leading to high rate of electron-hole recombination which results in slow reaction rates and reduced efficiency. The proposed design (Fig. 2(a)) has been aimed to manipulate in-plane electric-potential gradient in the optofluidic system via *in-situ* generation of self-powered micro-photogalvanic cells able to drive light-excited electrons from oxygen-starving reaction sites to the triple-phase boundary (oxygen gas-liquid reactant-solid photocatalyst) via electron-transport media. In this way, a larger proportion of photoactive sites can benefit from low recombination rates and improved photocatalytic performance.

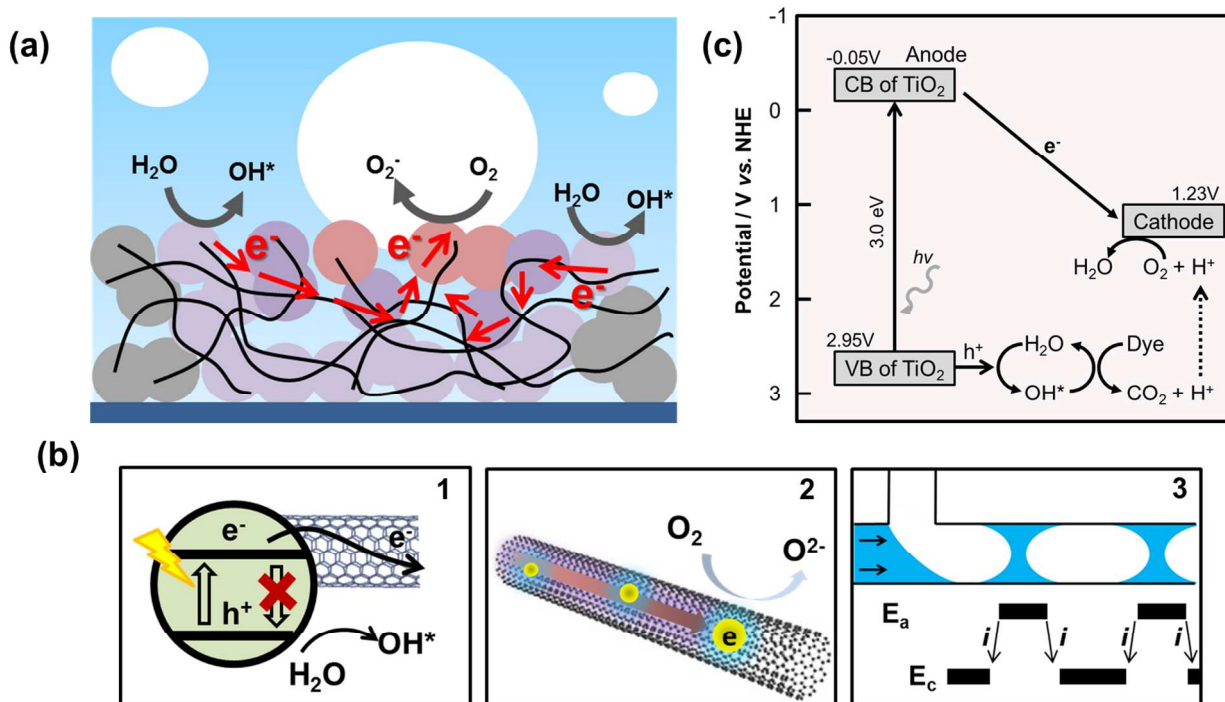


**Fig. 2.** Photogalvanic principle. (a) Principle of in-plane photogalvanic current generation between anodic and cathodic regions in photocatalyst layer. In the figure, the coloured balls at the bottom represent photocatalytic particles and the black curves represent electron transport media such as CNT; (b) key design elements enabling self-powered photogalvanic acceleration of optofluidic kinetics, which are (1) TiO<sub>2</sub>-CNT hybrid material for effective electron separation, (2) CNT matrix for fast electron transport, and (3) microfluidics for generating periodical O<sub>2</sub> concentration profile; and (c) Thermodynamics of microscale photogalvanic cells, in which  $i$  is the photo-induced current flowing between the anodic and cathodic region, and  $E_a$  and  $E_c$  are electric potential (V) the anodic and cathodic region, respectively.

A new paradigm for advanced photocatalytic technologies is then proposed based on three key design elements at both material and reactor levels as shown in Fig. 2 (b). These include (1) a photocatalyst material (TiO<sub>2</sub>-carbon nanotubes, CNT) was designed based on fundamental

understanding to promote the electrochemical kinetics of micro-photogalvanic cells. The TiO<sub>2</sub>-CNT Schottky barrier junction provides effective electron separation rate under light illumination [23]; (2) a fast electron transport can be achieved by integrating CNT as part of the photocatalytic material [24]. CNT could also serve as a good electrocatalyst to effectively promote oxygen reduction reactions [25]; and (3) dynamic and periodical O<sub>2</sub> concentration profile in the reaction system can be generated by adjusting shear/surface tension interactions at a T-junction microchannel. The manipulated dissimilar electrolyte environment could generate periodically-distributed equilibrium potential gradient between redox reactions and at the catalyst surface, similar to those in corrosion cells [26], driving the current between anodic and cathodic regions in the catalyst layer. In the present redox system, the anodic reaction is the photoelectrochemical oxidation of methylene blue (MB) while the oxygen reduction reaction (ORR) is the cathodic reaction. The proposed working principle is illustrated in Fig. 2 (c).

The significance of the proposed design is that it enables self-organization of numerous micro-photogalvanic cells, leading to photoelectrochemical synergetic effects in the optofluidic reactor without the need for an artificial two-electrode infrastructure and additional electric energy input. A schematic representation of the advanced optofluidic reactor is presented in Figure 3(a). A multiphase microchannel is integrated into the reactor by placing the immobilized photocatalyst layer at the bottom, with the light source on top (see also ESI). The degradation of methyl blue (MB) under UV-A illumination was selected as proof-of-concept of the system due to its previous extensive studies in optofluidic research [12, 15, 16, 19], which allows a fair comparison between these results and literature published experimental data. The photocatalytic degradation of MB is multi-step complex processes which can be explained by Langmuir–

Hinshelwood kinetics. Normally, the overall reaction rate constant [5] is used at the device level to evaluate the efficiency of reactors, in which the rate of dye decolourization is adopted. First-order kinetics model is the mostly commonly-acceptable and widely-used model for photocatalytic system operating at normal conditions. According to first-order kinetics law, the overall reaction rate constant of the microfluidic reactor is derived by

$$k = \frac{-\ln(1-x)}{t} \quad (1)$$

where  $k$  stands for the overall reaction rate constant ( $\text{s}^{-1}$ ),  $x$  is the decolourization percentage of the reactants and  $t$  is the effective residence time (s). Such evaluation system is predominately adopted in optofluidic reactor research, allowing a qualitative comparison among various reactor designs, even with different types of organic dyes and operation conditions.

Following multiphase microfluidic principles well developed in literature [27, 28], a precise control of oxygen delivery via T-junction microchannel can be achieved to form micro-bubbles by shear forces (Fig. 3(b), see also video record in ESI). Benefiting from the novel self-powered photogalvanic acceleration mechanism, the present optofluidic reactor was able to achieve a maximum reaction rate constant of  $1.32 \text{ s}^{-1}$ , with real-time features under UV-A illumination at room temperature. The reported optofluidic kinetics data are an order of magnitude superior to literature values for aqueous photocatalysis (Fig. 1(c)).

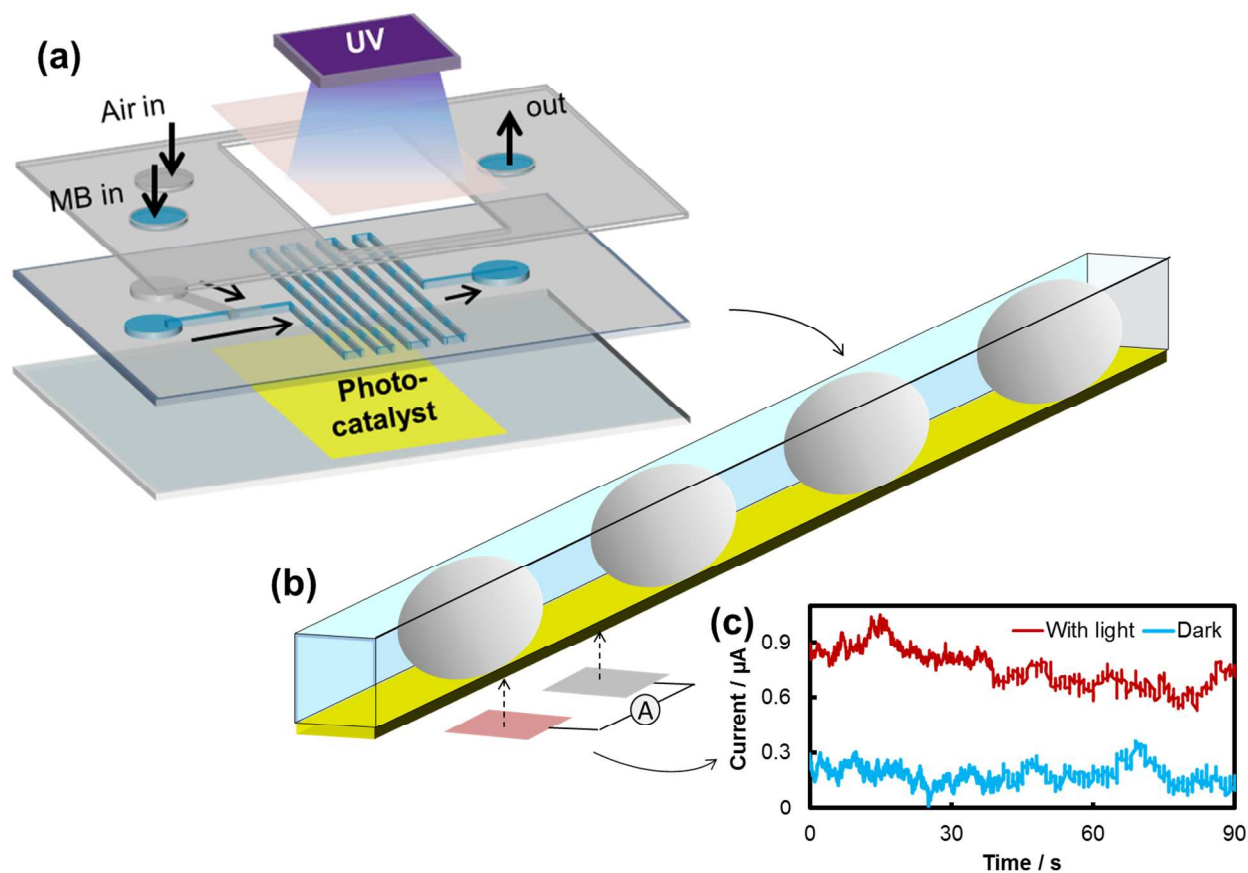


**Fig. 3.** Optofluidic reactor design. (a) Schematic of multiscale-designed optofluidic reactor; (b) schematic of the two-phase flow in the reactor; and (c) in-situ photogalvanic current measurement, including the current-time curves taken in both illuminated and dark conditions.

The presence of the photogalvanic current was demonstrated and measured in a specially-designed reactor (Figure 3 (b) and (c)), which shares identical geometric and operating parameters utilised in general performance tests, with the simple addition of two extra micro-electrodes integrated at the bottom of the  $\text{TiO}_2$ -CNT layer. The two micro-electrodes were connected to an external electrochemical station (CHI 660E), allowing measurements of electric current flowing in between the electrodes (more details on the measurement setup can be found in ESI). A significant photo-current was induced during illumination of the reactor, as compared

to no obvious current measured in the absence of UV-A light (Figure 3 (c)). A variation in photo-current can be observed in the current-time curves because the refresh of the surface by plug flow induces unsteady factors to the system. The direct measurement of *in-plane* photo-current at the micro-scale thus confirmed the existence of micro-photogalvanic cells in the optofluidic reactor.

The nanoscale TiO<sub>2</sub>-CNT hybrid photocatalyst was subsequently characterized as shown in Fig. 4. Fig 4(a) depicted the morphology of TiO<sub>2</sub>-CNT characterised by Scanning Electron Microscopy (SEM). CNT formed a disordered porous matrix that could serve as fast electron transfer network. TiO<sub>2</sub> nanoparticles were found to be embedded in the CNT porous network. Elemental mapping in Fig. 4(b) demonstrated a homogeneous distribution of C, Ti and O within the entire observed area of the hybrid film, indicating the formation of an uniform TiO<sub>2</sub>/CNT nanocomposite. Transmission Electron Microscopy (TEM) images (Fig. 4(c)) further confirmed the presence of embedded TiO<sub>2</sub> onto the CNTs, forming Schottky barrier heterojunction. Nanoparticle sizes were around 10 nm and 60 nm for TiO<sub>2</sub> and CNT, respectively. The inset of Fig. 4(c) shows an enlarged image taken nearby a heterojunction between TiO<sub>2</sub> nanoparticles and CNT. The interplanar spacing of 0.35 nm can be indexed to (101) planes of anatase TiO<sub>2</sub>. X-Ray Diffraction (XRD) patterns of CNT and TiO<sub>2</sub>-CNT hybrid thin films presented in Fig. 4(d) further confirm the planes of anatase TiO<sub>2</sub> phase (25.3°, 27.8°, 48.0°, 53.9°, 55.1° and 62.7° correspond to (101), (004), (200), (105), (211) and (204) [30]. Two peaks at 27.3° and 44.1° correlated to C(100) and C(002) planes of the CNTs [29] were also found in CNT and TiO<sub>2</sub>-CNT. The high intensity of such diffraction lines in the XRD patterns indicate a high crystallinity of the film after annealing at 450 °C.

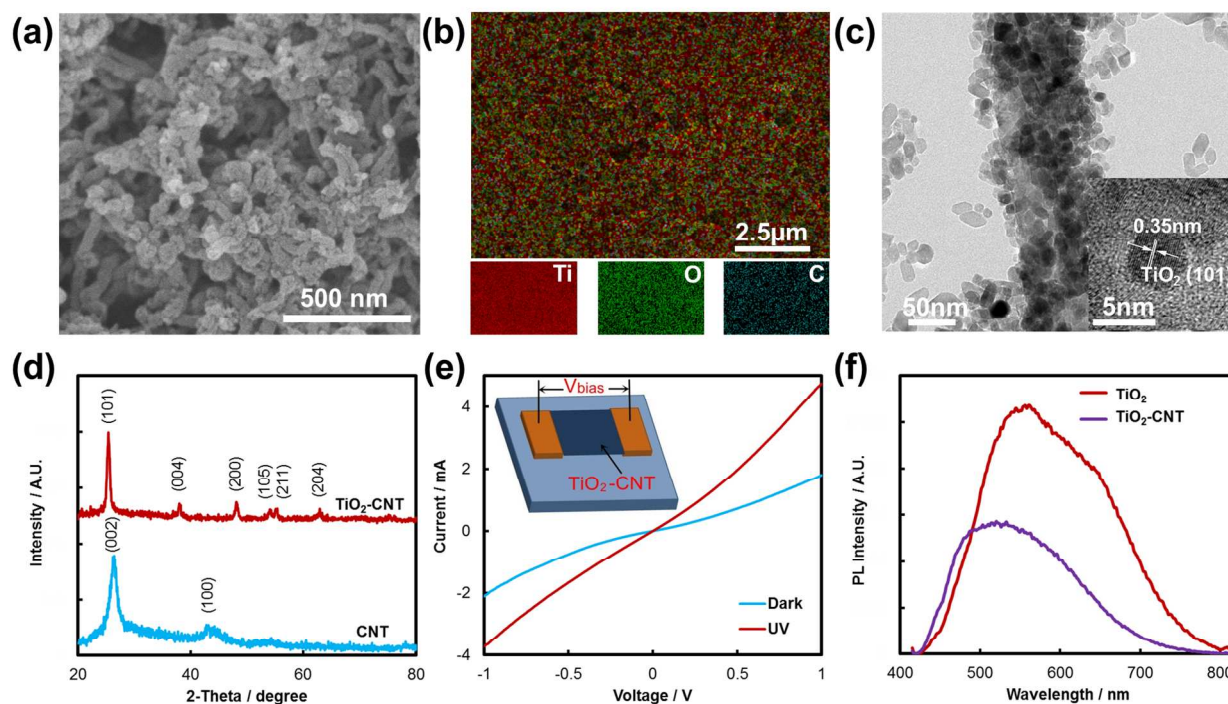


**Fig. 4.** Material characterization. (a) Top-view SEM image of  $\text{TiO}_2$ -CNT hybrid film obtained by mixing 35mg CNT with  $\text{TiO}_2$  paste and then sintering at  $450^\circ\text{C}$  for 30min in air; (b) Ti, O and C elemental mapping of  $\text{TiO}_2$ -CNT hybrid film; (c) TEM images of  $\text{TiO}_2$  nanoparticle attached CNT. Inset shows the enlarged image taken nearby a heterojunction; (d) XRD patterns of CNTs and  $\text{TiO}_2$ -CNT hybrid films. (e) Current-voltage curves of the  $\text{TiO}_2$ -CNT hybrid film under a bias of 1 V in the dark and light ( $2 \text{ mW cm}^{-2}$ ), respectively. Inset shows the device setup; (f) Photoluminescence spectra of pure  $\text{TiO}_2$  and  $\text{TiO}_2$ -CNT hybrid film.

To investigate the electron separation and transport capacity of the photocatalytic system, we configured a two-probe device for photo-electro-response test by contacting the two sides of the  $\text{TiO}_2$ -CNT film and scanning the voltage from  $-1$  to  $1$  V (inset of Fig. 4(e)). Typical current-voltage curves with and without UV illumination are shown in Fig. 4(e). The

significantly increased slope of the curve (43%) under light excitation revealed the generation of additional photo-electrons transferred from TiO<sub>2</sub> nanoparticles to CNT [31]. The strong correlation between the current and voltage variation also indicated a good conductivity of the hybrid thin film with minimal ohmic resistance. Furthermore, as shown in Fig. 4(f), in the presence of CNT the photoluminescence signal undergoes an obvious decrease in intensity, indicating the electron-hole recombination rate is significantly inhibited. A blue shift is also observed, evidencing the formation of Schottky barrier heterojunction. This further confirms that both electron separation and transport enhancement can be simply achieved via better material design. The PL results are in consistent with previous findings of similar TiO<sub>2</sub>-CNT materials, in which decrease in signal intensity and blue shift were observed as well [32].

Fig. 5 illustrates the self-powered photogalvanic accelerated performance (reaction rate enhancement by the newly-discovered photogalvanic effect) of the advanced photocatalytic system under different design and operation conditions. The effect of CNT amount in the TiO<sub>2</sub>/CNT hybrid material on the degradation performance was examined in Fig. 5(a). A maximum reaction rate constant of 0.53 s<sup>-1</sup> could be achieved with optimum quantities of CNT in the nanocomposite, namely 36 mg (i.e. 6.7 wt%). A low CNT content in the catalyst film could not maintain a sufficient carrier separation rate or provide a fast electron transport network, while excessive CNT may reduce the extent of irradiation at the titania active sites. Fig. 5(b) further shows the effect of gas-liquid (G/L) flow volume ratio on first-order reaction rate constant (*k*) and degradation rate. In the test, the G/L ratio varied by adjusting gas flow rates from 40 mL min<sup>-1</sup> to 470 mL min<sup>-1</sup>, under a constant liquid flow rate at 16 mL min<sup>-1</sup>. The reaction rate constant was found to increase at increasing G/L ratio up to a maximum value. For complete MB oxidation, the stoichiometric MB:oxygen ratio was 1:26, indicating serious oxygen

starvation in the reaction system. Increasing the oxygen supply rate will consequently benefit both photo-degradation as well as *in-situ* generated photogalvanic effects by avoiding the mass transport restraint from the cathodic side. Under optimised conditions (G/L ratio of 29:1 and residence time of 1.05 s), a maximum reaction rate constant of  $1.32 \text{ s}^{-1}$  was achieved, an order of magnitude superior to those of previous reported values for aqueous photocatalytic processes. However, the reaction residence time decreases with an increase in G/L ratio, leading to insufficient contact time between the reactant and the photocatalytic surface, and resulting in a decline in the degradation rate for a single pass.

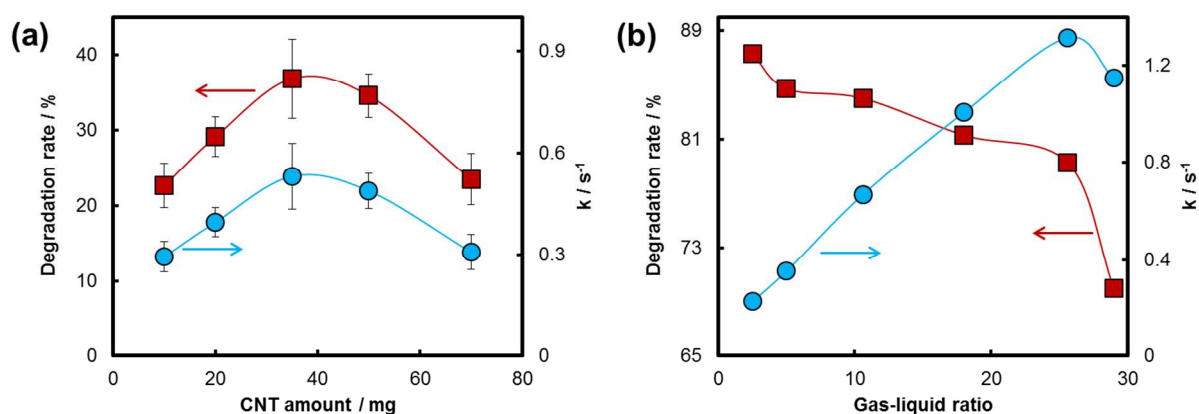


**Fig. 5.** Degradation percentage and reaction rate constant with respect to (a) different CNT amount, and (b) different gas-liquid ratios of the methylene blue solution in the reaction chamber.

A series of experiments were then conducted in order to confirm the remarkable contribution from the *in-situ* generated photogalvanic effect as well as the observed synergy between  $\text{TiO}_2$ -CNT and the multiphase optofluidic reactor design. The reaction rates of four sets of cases under the same geometric design and contact time were compared, namely (a) a single-phase flow reactor with  $\text{TiO}_2$ , (b) a multiphase flow reactor with  $\text{TiO}_2$ , (c) a single-phase flow reactor

with TiO<sub>2</sub>-CNT, and (d) a multiphase flow reactor with TiO<sub>2</sub>-CNT. The adoption of either multiphase flow design or the use of TiO<sub>2</sub>-CNT as photocatalytic hybrid material did not effectively improve the photo-degradation performance as compared to the control experiment (single-phase flow reactor using a pure TiO<sub>2</sub> photocatalyst, Figure 6). These findings were in good agreement with previous findings which proved the use of TiO<sub>2</sub>-CNT photocatalyst or multiphase reactor design shows rather limited effect on performance improvement in aqueous photocatalytic systems in certain circumstances [33, 34].

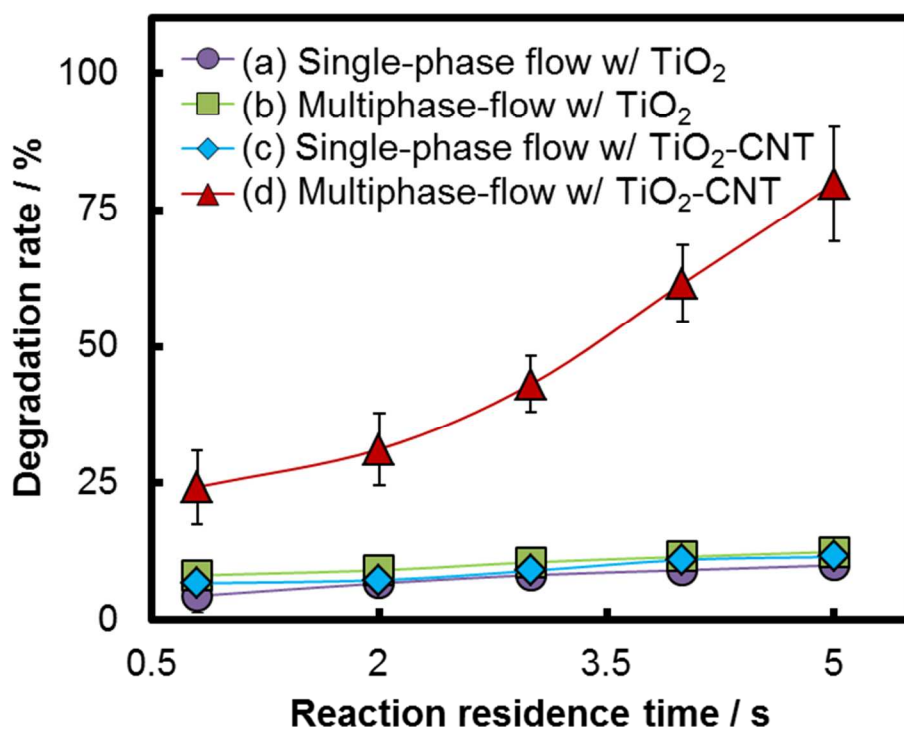


**Fig. 6.** The degradation rates of four sets of cases with respect to different effective residence times under the same geometric design. (1) single-phase flow reactor with TiO<sub>2</sub> photocatalyst, (2) multiphase flow reactor with TiO<sub>2</sub> photocatalyst, (3) single-phase flow reactor with TiO<sub>2</sub>-CNT hybrid photocatalyst, and (4) multiphase flow reactor with TiO<sub>2</sub>-CNT hybrid photocatalyst.

Mass-transfer intensification induced by the two phase flow system (by increasing the convective flux of MB to the reactive surface) did not show obvious performance enhancement, as the transport issue is generally not a limiting factor under optofluidics. It is also proved that increasing in the O<sub>2</sub> concentration by adding O<sub>2</sub> gas is also not the main reason for reaction rate boost as clearly indicated in Fig. 6. Comparatively, the combination of a multiphase flow reactor with a TiO<sub>2</sub>-CNT hybrid photocatalyst (proposed new generation advanced optofluidic system) exhibited a significantly enhanced performance to that of the control experiment. The results support the fact that the ultrafast kinetics can be attributed to the synergy between the advanced photocatalytic material and designed reactor across different length-scales.

The initial data presented here for the *in-situ* generated photogalvanic accelerated optofluidic reactor suggests that ultrafast reaction rates and real-time reaction features can be achievable in such photocatalytic systems. The advantage of the proposed optofluidic design principles relates to a remarkably improved performance even with simple catalytic materials and reaction engineering.

Several opportunities to improve the proposed first generation of advanced optofluidic photocatalytic technologies remain to be investigated. Firstly, a UV-A light source has been utilised in this study for the simple purpose of parameter control. TiO<sub>2</sub>-CNT has already showed a promising response under visible light irradiation (Fig. S1 in ESI), indicating a potential applicability of the present system under solar energy. Prototyping such a solar-responsive optofluidic reactor will be promising and could largely enhance its practical significance. In any case, the optofluidic reactor demonstrated in this study remains largely unoptimized. Multiscale parameters including reactor geometry, photocatalytic structure and composition as well as multiphase hydrodynamics are currently under investigation for optimum capabilities.

## Conclusions

This work represents a significant advance on the state of the art of aqueous-phase photocatalytic reactors. We have demonstrated that an appropriate photocatalyst design with an understanding of the optofluidic system and transport behavior at different scales, can lead to improved photocatalytic kinetics induced by an in-situ generated photogalvanic effect. The present optofluidic reactor achieves reaction kinetics in the time-scale of second using the most ordinary photocatalyst and normal reactor geometry without any need for costly and complex fabrication, synthesis, external field or high temperature operation. To the best of our knowledge, the data presented here represents the highest overall reaction rate constant, an order of magnitude faster to those observed in various types of aqueous-phase photocatalytic reactors. The use of our design principles are envisaged to pave the way to several opportunities and developments in photocatalytic system innovation, with new directions and possibilities towards low-cost, large-scale, high performance photocatalytic reaction systems.

## Acknowledgements

The research work is sponsored by National Basic Research Program of China (2014CB748500), Shanghai Pujiang Program (12PJ1402100) and Young Teachers Program of Universities in Shanghai (ZZHLG12012). RL gratefully acknowledges funding from Consejería de Ciencia e Innovación, Junta de Andalucía under project P10-FQM6711.

## References

- 1 A. Mills, R. H. Davies and D. Worsley, *Chem. Soc. Rev.* 1993, **22**, 417-425.
- 2 H. Harada, C. Hosoki, and A. Kudo, *J. Photochem. Photobiol. A* 2001, **141**, 219-224.
- 3 Y. Li, W. Xie, X. Hu, G. Shen, X. Zhou, Y. Xiang, X. Zhao and P. Fang, *Langmuir* 2009, **26**, 591-597.
- 4 A. Vaseashta, M. Vaclavikova, S. Vaseashta, G. Gallios, P. Roy and O. Pummakarnchana, *Sci. Technol. Adv. Mater.* 2007, **8**, 47-59.
- 5 L. Lei, N. Wang, X. M. Zhang, Q. Tai, D. P. Tsai and H. L. W. Chan, *Biomicrofluidics* 2010, **4**, 043004 .
- 6 N. Wang, X. Zhang, Y. Wang, W. Yu and H. L. W. Chan, *Lab Chip* 2014, **14**, 1074-1082.
- 7 Y. L. Chen, L. C. Kuo, M. L. Tseng, H. M. Chen, C.-K. Chen, H. J. Huang, R.-S. Liu and D. P. Tsai, *Opt. Express* 2013, **21**, 7240-7249.
- 8 W. Liu, M. Ji, and S. Chen, *J. Hazard. Mater.* 2011, **186**, 2001-2008.
- 9 X. Hao, H. Li, Z. Zhang, C. Fan, S. Liu and Y. Sun, *Chem. Eng. Res. Des.* 2009, **87**, 1604-1611.
- 10 J. Lv, W. Gong, K. huang, J. Zhu, F. Meng, X. Song and Z. Sun, *Superlattices Microstruct.* 2011, **50** , 98-106.
- 11 Q. R. Deng, X.H. Xia, M.L. Guo, Y. Gao and G. Shao, *Mater. Lett.* 2011, **65**, 2051–2054.
- 12 A. Pourahmad. S. Sohrabnezhad and E. Kashefian, *Spectrochim Acta A.* 2010, **77**, 1108–1114.
- 13 N. Wang. L. Lei, X.M. Zhang, Y.H. Tsang, Y. Chen and H.L.W. Chan, *Microelectron. Eng.* 2011, **88**, 2797–2799.
- 14 Z. Meng, X. Zhang and J. Qin, *Nanoscale* 2013, **5**, 4687-4690.
- 15 N. Wang, X. Zhang, B. Chen, W. Song, N.Y. Chan and H.L. Chan, *Lab Chip* 2012, **12**, 3983–3990.

- 16 L. Li, R. Chen, X. Zhu, H. Wang, Y. Wang, Q. Liao and D. Wang, *ACS Appl. Mater. Interfaces* 2013, 5, 12548–12553.
- 17 Z. He, Y. Li, Q. Zhang, H. Wang, *Appl. Cat. B*. 2010, 93, 376–382.
- 18 H.C. Aran. D. Salamon, T. Rijnaarts, G. Mul, M. Wessling and R.G.H. Lammertink, *J. Photochem. Photobiol. A*. 2011, 225, 36– 41.
- 19 H. Zhang, J.-J. Wang, J. Fan and Q. Fang, *Talanta* 2013, 116, 946-950.
- 20 C.-H. Wu, & J.-M. Chern, *Ind. Eng. Chem. Res.* 2006, 45, 6450-6457.
- 21 M. J. Uddin, M. M. Alam, M. A. Islam, S. R. Snigda, S. Das, M. M. Rahman, M. N. Uddin, C. A. Morris, R. D. Gonzalez, U. Diebold, T. J. Dickens and O. I. Okoli, *Intl. Nano Letters* 2013, 3, 1-10.
- 22 M. H. Reed, *Geochim. Cosmochim. Acta* 1982, 46, 513-528.
- 23 M. R. Hoffmann, S. T. Martin, W. Choi, and D. W. Bahnemann, *Chem. Rev.* 1995, 95, 69-96.
- 24 W. Wang, P. Serp, P. Kalck, and J. L. Faria, *J. Mol. Catal. A*. 2005, 235, 194-199.
- 25 K. Gong, F. Du, Z. Xia, M. Durstock and L. Dai, *Science* 2009, 323,760-764.
- 26 B. F. Brown, *Corrosion* 1970, 26, 349-350.
- 27 D. Qian, and A. Lawal, *Chem. Eng. Sci.* 2006, 61, 7609-7625.
- 28 T. Nisisako, T. Torii, and T. Higuchi, *Lab Chip* 2002, 2, 24-26.
- 29 A. Cao, C. Xu, J. Liang, D. Wu, and B. Wei, *Chem. Phys. Lett.* 2001, 344, 13-17.
- 30 Y. Jun, M. F. Casula, J.-H. Sim, S. Y. Kim, J. Cheon and A. P. Alivisatos, *J. Am. Chem. Soc.* 2003, 125, 15981-15985.
- 31 E. Shi, L. Zhang, Z Li, P. Li, Y. Shang, Y. Jia, J. Wei, K. Wang, H. Zhu, D. Wu, S. Zhang and A. Cao, *Sci. Rep.* 2012, 2, 884.

32. M. Barberio, P. Barone, A. Imbrogno, S. A. Ruffolo, M. L. Russa, N. Arcuri and F. Xu, *J. Chem. Chem. Eng.* 2014, 8, 36-41/
- 33 W. J. Lee, J. M. Lee, S. Thomas Kochuveedu, T. H. Han, H. Y. Jeong, M. Park, J. M. Yun, J. Kwon, K. No, D. H. Kim, and S. O. Kim, *ACS Nano* 2011, 6, 935-943.
- 34 H. Lindstrom, R. Wootton and A. Iles, *AIChE J.* 2007, 53, 695-702.

**Electronic Supplementary Information (ESI)****Self-powered photogalvanic acceleration of optofluidic kinetics: a new paradigm for advanced photocatalytic technologies**

Huizhi Wang <sup>a</sup>, Xiaojiao Luo <sup>bd</sup>, Michael K.H. Leung <sup>c</sup>, Dennis Y.C. Leung <sup>b</sup>, Zhiyong Tang <sup>d</sup>,  
Hailiang Wang <sup>e</sup>, Rafael Luque <sup>f</sup>, Jin Xuan <sup>a\*</sup>

<sup>a</sup> School of Engineering and Physical Sciences, Heriot-Watt University, Edinburgh, United Kingdom

<sup>b</sup> Department of Mechanical Engineering, The University of Hong Kong, Pok Fu Lam, Hong Kong

<sup>c</sup> Ability R&D Energy Research Centre, School of Energy and Environment, City University of Hong Kong, Tat Chee Avenue, Kowloon, Hong Kong

<sup>d</sup> CAS Key Laboratory of Low-Carbon Conversion Science and Engineering, Shanghai Advanced Research Institute, Chinese Academy of Sciences, Shanghai 201210, China

<sup>e</sup> Department of Chemistry, Yale University, West Haven, CT, United States

<sup>f</sup> Departamento de Química Orgánica, Universidad de Córdoba, Edif. Marie Curie, Ctra Nnal IV-A, Km 396, E14014 Córdoba, Spain

\*Corresponding Author, Tel: +44 (0) 131 449 5111; Fax: +44 (0)131 451 3136. Email addresses:

j.xuan@hw.ac.uk (J. Xuan).

\*Corresponding Author, Tel: +44 (0) 131 449 5111; Fax: +44 (0)131 451 3136. Email addresses: j.xuan@hw.ac.uk (J. Xuan).

## 1. Experimental details

**Material.** Prior to coating process, normal glasses (Xin Yan Technology Ltd.) were cut into 3.5cm×3.5cm squares and cleaned by sonication in ethanol. The TiO<sub>2</sub>-CNT paste was prepared via the following procedures. 2g multi-walled CNT (95%, Chengdu Organic Chemicals Co. Ltd.) was added into a mixture of 125ml HNO<sub>3</sub> (70%, Sigma-Aldrich) and 375ml H<sub>2</sub>SO<sub>4</sub> (95-97%, Sigma-Aldrich) and sonicated for surface treatment. To remove the amorphous carbon species, the treated CNTs were then heated at 400°C in air. The obtained CNTs were mixed with 0.5g TiO<sub>2</sub> paste (20nm, DHS-TPP3, HeptaChroma Ltd.) and grinded in a mortar. Different CNT/TiO<sub>2</sub> composite films were prepared with varying TiO<sub>2</sub>/CNT amount ratio to adjust the material properties. Then, doctor-blading method was used to coat the mixture paste on the glass with controlled film thickness of 5.15 μm. Consequently the film-coated glass was dried at 100°C for 4 min in air. The obtained sample was further annealed at 450°C for 30 min in a muffle furnace to remove the organic additives and to form porous matrix structures. FE-SEM (Hitachi S4800), TEM (FEI Tecnai G2 20) and XRD (Philips X'pert) using Cu K α radiation ( $\lambda = 1.5418 \text{ \AA}$ ) with an operating voltage of 40 kV and a current of 30 mA were used to characterize the material morphology and properties.

**Reactor fabrication.** The T-junction microchannel was fabricated on a 0.1-mm thick PMMA sheet by a CO<sub>2</sub> laser system (Universal). The dimensions of the serpentine microchannel are 141.77 mm×0.1 mm×0.6 mm ( $l \times w \times h$ ) with total volume of 8.5  $\mu$ L. Inlet and outlet holes (3 mm in diameter each) and a square window (18 mm×18 mm) for quartz placement are processed on another piece of PMMA placing on top of the microchannel layer. The CNT/TiO<sub>2</sub> coated glass is adhered to the bottom of the microchannel layer to form an enclosed reaction system. The effective catalyst/illumination area is 14.18 mm<sup>2</sup>.

**Test and control.** A 365 nm wavelength UV-A lamp (Cole Parmer 9815) was used as the light source under the illuminate intensity of 2 mW cm<sup>-2</sup>. Two syringe pumps are used to control the liquid and gas flow in the optofluidic reactor separately. By adopting different gas/liquid flow ratio, different multiphase flow patterns are generated. At outlet, the exiting reactant liquid was collected and then sent to a UV-vis spectrophotometer (Shimadzu, UV-1800) for MB concentration measurement, based on which, degradation rate and reaction rate constant are calculated. Current-voltage curves of the TiO<sub>2</sub>-CNT hybrid film is measured by two-probe method with an electrochemical station (CHI 660). Photoluminescence (PL) spectra of the thin-film materials are recorded at room temperature using a spectrofluorophotometer (Shimadzu, RF-5301). To provide direct evidence on the proposed photogalvanic effect in our multiscale design, a specially-designed reactor is fabricated to perform in-situ photoelectrochemical characterization. The reactor is designed to share the same geometric and operating parameters used in general test, except that two extra micro-electrodes are integrated at the bottom of the TiO<sub>2</sub>-CNT layer, with interval at the same length-scale of a single micro-photo-galvanic cell.

The two micro-electrodes are connected to an external electrochemical station (CHI 660E). Therefore, electric current flowing in between the electrodes can be captured.

## 2. UV-vis absorption spectra

Fig. S1 shows the UV-vis absorption spectra of  $\text{TiO}_2$  with and without CNT additives. The spectrum taken for a pure  $\text{TiO}_2$  film shows transparency for wavelengths above 370 nm. The  $\text{TiO}_2$ -CNT hybrid films show significant absorption in the visible range. The amount of  $\text{TiO}_2$  added also affect the material band gap significantly as the absorption spectrum taken from the sample with 25mg CNT exhibits obvious increase in the absorption in the visible light range compared to the one with 10 mg CNT.

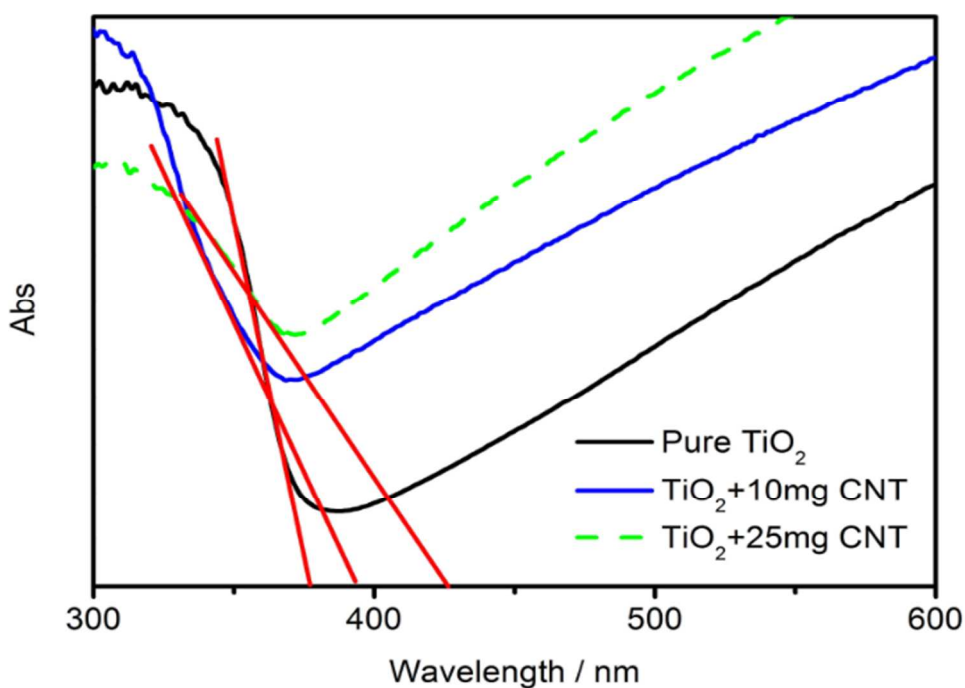


**Fig. S1.** UV-vis absorption spectra of  $\text{TiO}_2$  with and without CNT additives

